We are IntechOpen,
the world's leading publisher of
Open Access books
Built by scientists, for scientists

4,800
Open access books available

122,000
International authors and editors

135M
Downloads

Our authors are among the

154
Countries delivered to

TOP 1%
most cited scientists

12.2%
Contributors from top 500 universities

Interested in publishing with us?
Contact book.department@intechopen.com

Numbers displayed above are based on latest data collected.
For more information visit www.intechopen.com

Sintering Processing of Complex Magnetic Ceramic Oxides: A Comparison Between Sintering of Bottom-Up Approach Synthesis and Mechanochemical Process of Top-Down Approach Synthesis

Zhi Huang Low, Ismayadi Ismail and Kim Song Tan

Additional information is available at the end of the chapter

Abstract

Sintering is a common synthesis method for the fabrication of ceramics. The widespread use of sintering for the production of complex ceramic oxide especially ferrites has led to a variety of investigations on the subject. Top-down approach synthesis like mechanochemical process has recently been suggested as a promising synthesis method for replacing bottom-up approach synthesis methods like sintering, questioning its necessity for thermal treatment at high temperature. Understanding of sintering mechanism is crucial in order to optimize and enhance the advantages of sintering, which cannot be replaced by other techniques. In general, ferrites with particular set of behaviors require a particular set of microstructural properties influenced by the sintering steps. The main objective of this chapter is to understand how the increase of sintering temperature affects the microstructural evolution, in order to develop a fundamental science understanding for the mechanism of sintering. In the second part of this chapter, presentation of experimental results on sintering of mechanically activated $Ni_{0.5}Zn_{0.5}Fe_2O_4$ nanoparticles and its effect on microstructural, magnetic, and optical properties was reported. Lastly, a comparative study between sintering (bottom-up approach) and mechanochemical (top-down approach) process is presented.

Keywords: bottom-up approach, sintering, barium hexaferrite, Ni-Zn ferrite

1. Introduction

Sintering is one of the oldest material synthesis methods has existed for thousands of years. Since the introduction of controlled sintering process of ceramic, the methodology has gained

rapid growth and well established as one of the most trustable synthesis method for the production of complex ceramic oxides with desired properties [1]. Sintering is categorized as bottom-up approach synthesis as it involves the construction of nanostructures in materials atom-by-atom, layer-by-layer, from small to large sizes [2]. Since twentieth century, energy efficiency and productivity are two important factors in choosing a particular methodology [3]; therefore, top-down approach synthesis method like mechanochemistry has emerged as one of the most promising candidates to replace known current methodologies like sintering, questioning the necessity for thermal treatment at high temperatures. However, there are advantages of sintering that are irreplaceable by other methodologies. Sintering offers matter transport through diffusion while maintaining the stoichiometry of the ceramic material. Commonly, a single phase ceramic oxide with low porosity can be achieved by sintering of the material to a range of 50–80% of its melting point [1]. With an appropriate sintering temperature, the material does not melt, while atomic diffusion can be activated to achieve a dense, compact, and high crystallinity material, which is essential for the fabrication process. Although the optimization of sintering parameters to achieve complete phases of complex ceramic oxides is crucial; however, the fundamental knowledge behind sintering: the correlation between microstructural properties induced by the thermal activation of sintering, with important behaviors like magnetic and optical properties, is important for the understanding of sintering mechanism.

2. Microstructural aspects of complex magnetic ceramic oxides

Microstructure of complex magnetic ceramic oxides consists of grains, grain boundaries, porosity, and defects structures. As complex as it is microstructural properties influence the behaviors of these complex ceramic oxides. For instance, microstructural properties like surface morphology, atomic arrangement, size and shape affect major macroscopic properties such as magnetic, optical, mechanical, electrical, and many other properties of complex ceramic oxides. These are known as the microstructural dependent behaviors of complex ceramic oxides. Nanomaterials exhibit unique behaviors compared to their bulk counterparts [4].

2.1. Size

There are some important behaviors related to magnetic ceramic oxides, which are size dependent. For instance, magnetic properties and particle, grain, or crystallite size are relevant to each other. When the particles are in nano-size, the percentage of amorphous grain boundary volumes in material is high compared to particles in micron size. The presence of large volume fraction of amorphous phase in the material hinders the exchange interaction between magnetic moments. Therefore, small particles are likely to exhibit weak ferromagnetic, superparamagnetic, and paramagnetic behaviors. Small size polycrystalline nickel zinc ferrite dissipates minimum energy [5]. The magnetocrystalline anisotropy energy, E_A for ferrite can be defined by the following equation:

$$E_A = KV \sin^2 \Theta \tag{1}$$

where K is the anisotropy constant, V is the volume of the crystal, and Θ is the angle between the easy axis and the direction of the field-induced magnetic field. When the grains are small in dimensions or below a critical size, they dissipate minimum energy, therefore, the energy required to create a new domain or shifting the domains is much higher than that required in maintaining the material as single domain. The effect of grain size changed some aspects of magnetic behavior of yttrium iron garnets [6]. Below a critical size, as the volume or size of the grains increases, grain size remains in the single-domain range, therefore, the E_A value increases, the magnetocrystalline anisotropy energy becomes stronger and the coercivity (the energy required to change the direction of the magnetization) increases. After the grain size exceeds the critical size, intergranular domain walls are formed inside the grains, because the energy is not sufficient to maintain relatively big grains as single domains. Therefore, domain walls are created to reduce the overall energy of the system. Grain size has similar impact on the magnetic properties of hard ferrite, $BaFe_{12}O_{19}$, which has a critical size as well. Studies defined the critical size as the minimum grain volume that the anisotropy energy is able to overcome thermal agitation [7].

Another important magnetic behavior is the measure or ability of a material to sustain a magnetic field within the material when external field applied. This is known as the magnetic permeability. Magnetic permeability is strongly influenced by the presence of grain boundaries or amorphous surfaces, as they will act as impediments to domain wall movement. Bulk materials have fewer grain boundaries, therefore, higher the permeability. This phenomenon especially noticeable in ferrites as their grain boundaries are thicker [4]. The effect of sintering soaking time on the microstructural properties of nickel zinc ferrite was investigated [8, 9]. Grain size increases with increasing soaking time. The increase of grain size is the main factor that causes the increase of initial permeability. Bulk materials have a low-volume fraction of grain boundary as shown in **Figure 1**. Volume fraction can be represented by:

$$V_{shell} = \frac{\frac{4}{3}\pi R^3 - \frac{4}{3}\pi r^3}{\frac{4}{3}\pi R^3} \times 100\% \qquad (2)$$

where V_{shell} is the volume fraction of the structurally disordered boundary region, R is the radius of a particle, and r is the radius of the core region of a particle. If we assume the thickness of the shell
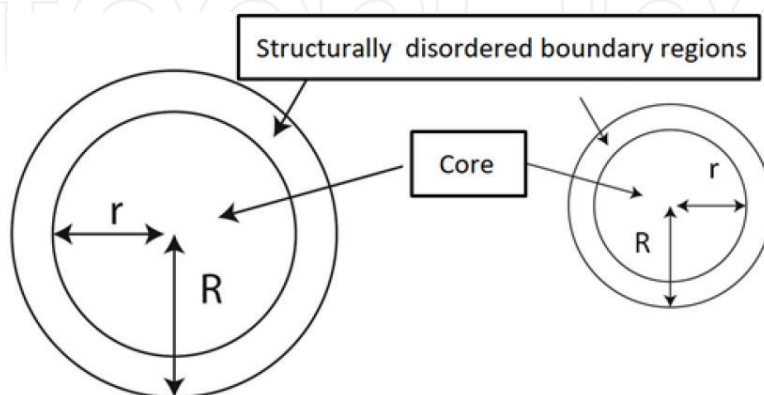

Figure 1. Schematic representation of bulk and nanoparticles, and the definition of R, radius of a particle, and r, radius of the core of a particle.

is approximately 5 nm, for nanoparticles (R < 100 nm), the volume fraction of this structurally disordered shell is large (>10%) while for bulk material, the volume fraction of the shell is not significant (<0.02%). As the particles undergo densification and coarsening through increasing sintering temperature, particle size increases from nano-sized to micron-sized. As a result, volume fraction of disordered grain boundary becomes less significant. Therefore, the pinning effects of this disordered boundary region on the domain walls motion is not significant for bulk materials.

2.2. Defects and porosity

Porosity is another microstructural feature that has the pinning effect on the movement of the domain walls. Porosity is abundant in complex magnetic ceramic oxide because it cannot be eliminated by heat treatment. Heat treatment offers grain growth, densification, and boundaries expansion. However, many pores are swept over by grain boundaries and remain within large grain [4]. Porosity and grain size effects sometimes seem inseparable because grain growth and densification happen simultaneously. In case of magnetic properties, saturation magnetization is associated with the following equation [10]:

$$M_s = (1 - p)\, 4\,\pi M_o \tag{3}$$

where p is the porosity, M_o is the magnetization extrapolated to zero porosity. Therefore, we can conclude that saturation magnetization is porosity dependent while coercivity is size dependent. Previous study proved that the independence of coercivity from porosity, while saturation magnetization and remanence are independent from grain size effect [10]. In addition to porosity, other defects such as cracks, inclusions, foreign phases, strains, as well as dislocations would alter the magnetic behaviors of ferrites. Defects act as energy wells have a strong pinning effect on the domain wall motion and thus require higher activation energy to detach [4].

2.3. Boundary region

It is believed that boundary region possesses higher energy compared to volume defects. Therefore, boundary region is a highly reactive region, which allows nucleation of new phases. As nanostructured materials have higher surface-to-volume ratio, they are reactive compared to their corresponding bulk materials. In ceramic materials, boundary region between phases and grains governs many properties and processes, for example, as fracture strength, plastic deformation, conductivity, dielectric loss, and phase transformation. All materials have interfacial energy and tension that can be calculated by same thermodynamic formulation [11]. Boundaries act as sinks and sources for the formation of lattice imperfections, diffusion, and phase transformations when deformation occurs. Some behaviors of ceramic oxides such as coercivity and permeability are strongly related to their boundaries [12]. The direction of magnetic moments within the material could be changed easily when the pinning effects of the boundary regions is diminished. Apparent permeability can be expressed as following [13]:

$$\mu_{app} = \frac{(1-p)\,\mu_o}{\left(1 + \frac{p}{2}\right)\left(1 + 0.75\,\frac{t}{D}\,\frac{\mu_o}{\mu_b}\right)} \tag{4}$$

where p is the porosity, D is the average grain size, t is the effective thickness of boundary region, μ_b is the permeability of the boundary region, μ_o is the permeability free form the demagnetizing

field. From the equation, notice that the thickness of boundary region has strong influence on the control of the magnetic properties of ferrites because the thickness of the boundary regions can be altered simply by small amount of additives, impurities, or phase transformations.

3. Ceramic synthesis techniques

Attention has been paid to investigate synthesis techniques and their impacts on new materials, particularly nanostructured and nanocrystalline materials. Synthesis technique is strongly related to behaviors of the investigated nanomaterial because the chosen synthesis technique is responsible for tailoring the atomic and microstructure of the nanostructured material. Numerous published studies have improved our understanding of the effects of synthesis technique on the behaviors of complex magnetic ceramic oxide, especially technologically important hard and soft ferrites [5, 14–16]. Most of the significant findings show that the results are of limited significance unless the microstructures, chemical composition, defects, and atomic arrangement of the investigated ferrite are well-characterized. Generally speaking, the techniques of preparing ferrite are categorized into two: bottom-up and top-down approaches, as shown in **Figure 2**. Bottom-up approach synthesis is a ceramic powder processing approach that engages atoms, ions, molecules or particles as starting building blocks.
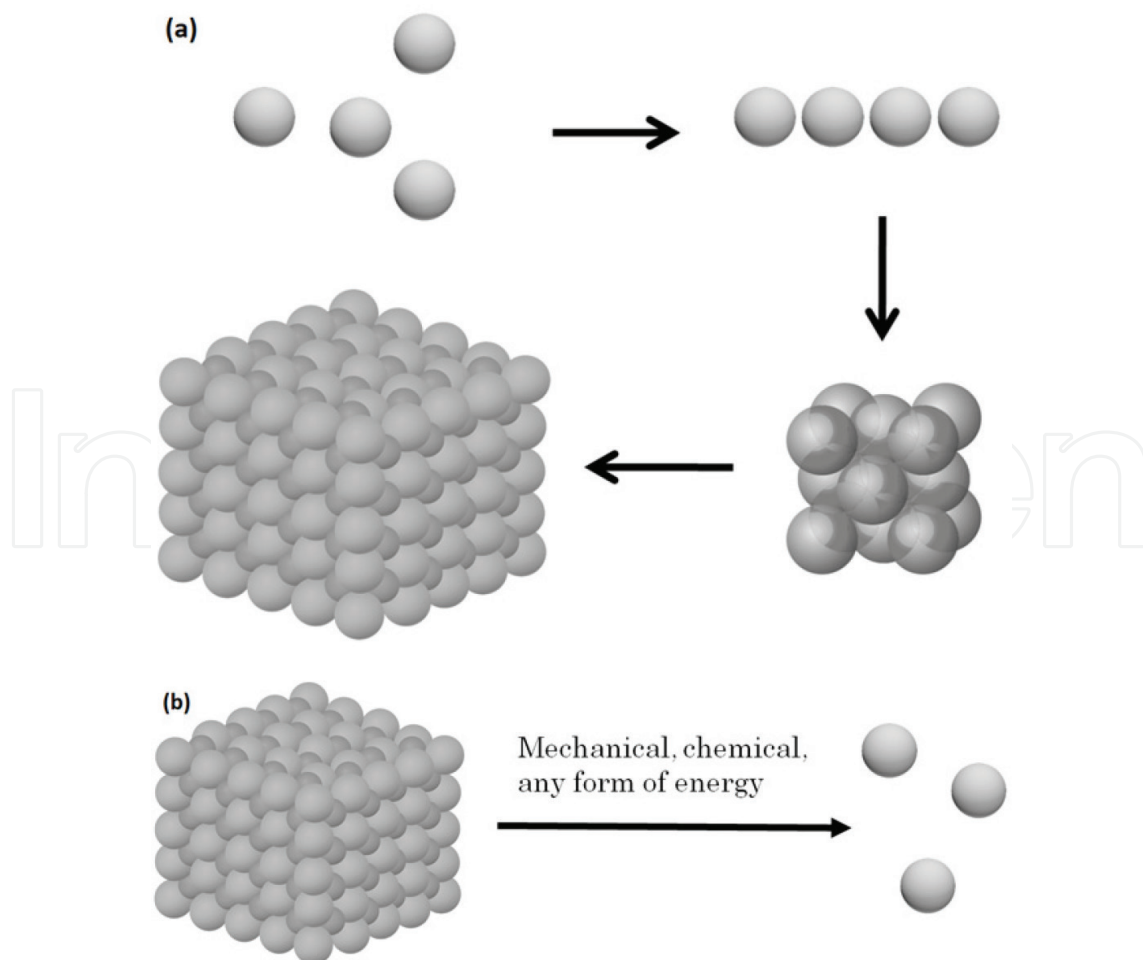

Figure 2. Schematic representations of (a) bottom-up and (b) top-down approaches.

By combining or assembling these building blocks, nanoscale clusters, or corresponding bulk materials are formed. Top-down approach synthesis is a ceramic powder processing approach that begins with micro-structured materials. The approach utilizes mechanical, chemical, or other form of energy to perform structural decomposition to obtain nanoscale materials. Both approaches have its advantages and drawback. For instance, bottom-up approach synthesis such as chemical processes and solid-state routes are capable of producing fine nanocrystalline materials with high purity and homogeneity. However, they have disadvantages like not environmental friendly, high cost of chemical precursors, solvent evaporation, and necessity for thermal treatment at high temperature. On the other hand, top-down approach synthesis like mechanochemical process is considered as green process because it minimizes damage to the environment, fast, economical, and can effectively take nanostructure forms [2]. However, contaminations, defects, and damages that were induced into the material system need to carefully take into account for good material production [15].

4. Ferrites

Ferrites belong to a class of complex magnetic ceramic oxide. The crystal structure of ferrites can be observed as an interlocking network of cations and negatively charged divalent oxygen ions [4]. When a layer of oxygen ions is closely packed lines that connect the centers of these oxygen ions will form a network of equilateral triangles. The second layer of closely packed oxygen ions is arranged in such a way that the centers of these oxygen ions are superimposed with the centers of the equilateral triangles of the first layer. If a similar third layer repeats the same arrangement with the first layer, this arrangement is known as hexagonal close-packed structure in the type of "ababab" stacking sequence. On the other hand, if the third layer arranges in such a way that the centers of the oxygen lie directly over the centers of equilateral triangles adjacent to the ones used for hexagonal close-packed, this will produce a cubic close-packed with a stacking sequence of "abcabc." Then, ferrites are further categorized according to their molar ratio of Fe_2O_3 to other oxide components (modifier oxide) present in the ceramic as presented in **Table 1**.

Type	Structure	Molar ratio of Fe_2O_3 to modifier oxide	Modifier oxide	Example
Magnetoplumbite	Hexagonal	6:1	Group IIA divalent metal oxide. Example: BaO, SrO	$BaFe_{12}O_{19}$
Spinel	Cubic	1:1	Transition metal oxide. Example: NiO, ZnO	$Ni_{0.5}Zn_{0.5}Fe_2O_4$
Garnet	Cubic	3:5	Rare earth oxide	$Y_3Fe_3(FeO_4)_3$

Table 1. Classification of ferrites according to variation in molar ratio of Fe_2O_3 to modifier oxide.

5. Sintering of mechanically activated ferrite powders

Top-down and bottom-up approaches have their own advantages and drawback as mentioned in the previous section. Conventional solid-state process is a bottom-up approach ceramic processing method that involves neither wet chemical reactions nor vapor phase interactions. There are two important processing steps that will affect the quality of the end product: starting powder preparation and heat treatment. The solid-state process is considered as the simplest synthesis route for various ferrites. In the starting powder preparation stage, high-purity raw materials would mix together according to the stoichiometric balance of the final product. This mixing process is being carried out by either dry or wet milling media for a certain period to produce a homogenous distributed starting powder. Then, the starting powder will undergo a heat treatment, typically with the use of a furnace to obtain the final product.

The conventional solid-state process is capable of producing advanced material with unique compositions such as refractory ceramics, glasses, and crystals. Previous research showed that conventional solid-state process was capable of producing particles between 100 nm and 1 micron [16]. However, conventional solid-state process may result in high synthesis temperature because diffusion reaction is limited under low temperature. Besides, this process may produce an incomplete reaction, which results in inhomogeneous products. Other issues of using this process are lack of control of the kinetics and the difficulties of producing desired end products [17]. In order to overcome the drawback of conventional solid-state process, the implementation of mechanical alloying in the starting powder preparation is recommended by many researchers. Apart from the practicality, mechanically activated starting powders exhibit nanostructures and high reactivity. Therefore, it provides an easy, fast, and economical option to produce the desired material. Previous studies showed that starting powder synthesized via mechanical alloying, had a relatively low sintering temperature for the formation of pure, single phase material [5, 7, 18, 19].

6. Experimental results of sintering of mechanically activated soft ferrite $Ni_{0.5}Zn_{0.5}Fe_2O_4$

6.1. Microstructural properties

X-ray Diffraction (XRD) spectra of $Ni_{0.5}Zn_{0.5}Fe_2O_4$ after sintering from 600 to 1200°C are presented in **Figure 3**. In view of the results obtained, the occurrence of [121] peak in 600°C spectrum indicated incomplete reaction between raw materials to form a single phase powder. α-Fe_2O_3 existed as secondary phase at 600°C. The [121] peak shows the existence of secondary phase α-Fe_2O_3 in the $Ni_{0.5}Zn_{0.5}Fe_2O_4$ phase. The α-Fe_2O_3 phase disappeared when the sintering temperature was increased to 700°C. A complete $Ni_{0.5}Zn_{0.5}Fe_2O_4$ was formed as Zn^{2+} ions diffused into the tetrahedral sites while Ni^{2+} ions occupied the octahedral sites. As the starting powders were mechanically activated by high-energy ball milling by SPEX is the modal name of the dual mixer machine. Which was specially modified to achieve high speeds (approximately 1725 rpm) for the effective production of nanostructured particles; this enables the
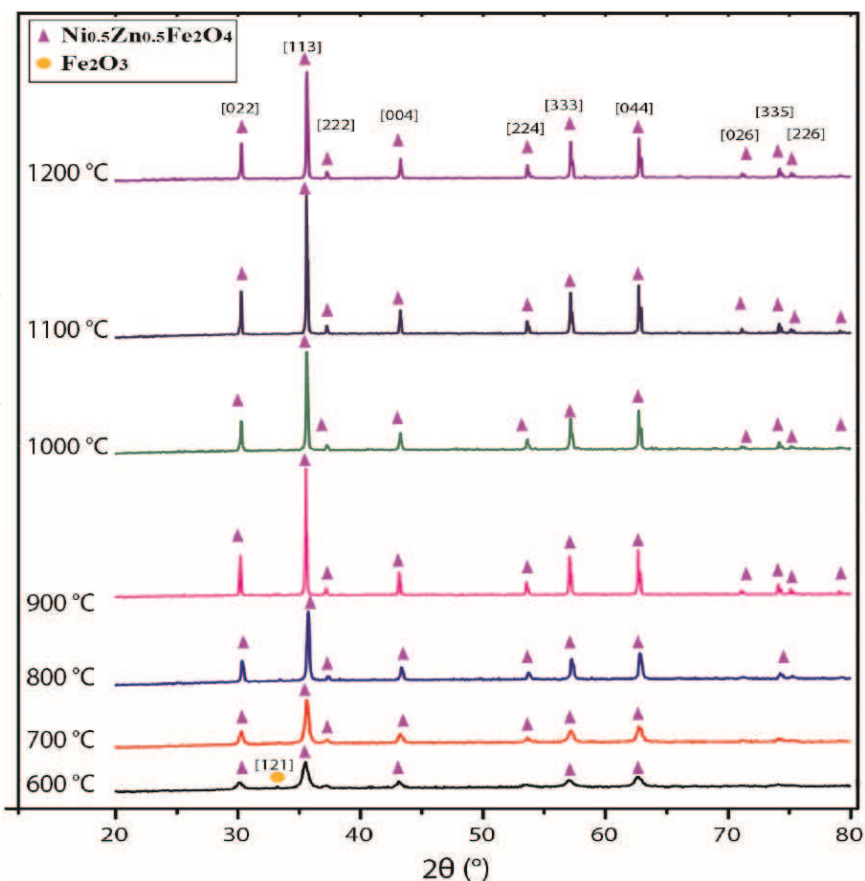
Figure 3. X-ray diffraction patterns of $Ni_{0.5}Zn_{0.5}Fe_2O_4$ sintered from 600 to 1200°C.

formation of single phase at a lower sintering temperature. It is worth mentioning that the synthesis temperature for single phase Ni-Zn ferrite for refluxing method is between 950 and 1150°C [20]; sol–gel technique requires more than 1000°C [21]; co-precipitation method requires 550–1000°C [22]. The intensity of the Bragg peaks increased, and the peak widths decreased with increasing sintering temperature indicating the increase of crystallinity and particle size.

Structural information was obtained from Rietveld refinement. The increase of lattice parameters and unit cell volume was observed. As shown in **Figure 4**, as the sintering temperature increased, the unit cell volume expanded, and Zn^{2+} ions diffused into the interstitial sites; this was crucial for the reaction as interstitial diffusion is the most important lattice diffusion mechanism [1]. Further increasing of sintering temperature (>900°C), a decrease in lattice parameters and unit cell volume was observed. This could be due to the small amount of Zn^{2+} ions evaporated from the lattice [8]. This is because zinc has a low-boiling point of 907°C. Mechanically activated starting material has high lattice strain as defects and inhomogeneity could be introduced into the system. This is known as the second order stress, which it modifies the materials by one grain to another or from one part of the grain to another on a microscopic scale. There was also first order stress induced by milling. This type of stress modifies the material uniformly across the entire material [23], causing a macroscopic variation on the material. By increasing the sintering temperature, relaxation can be attained for macro and micro stresses induced during milling.
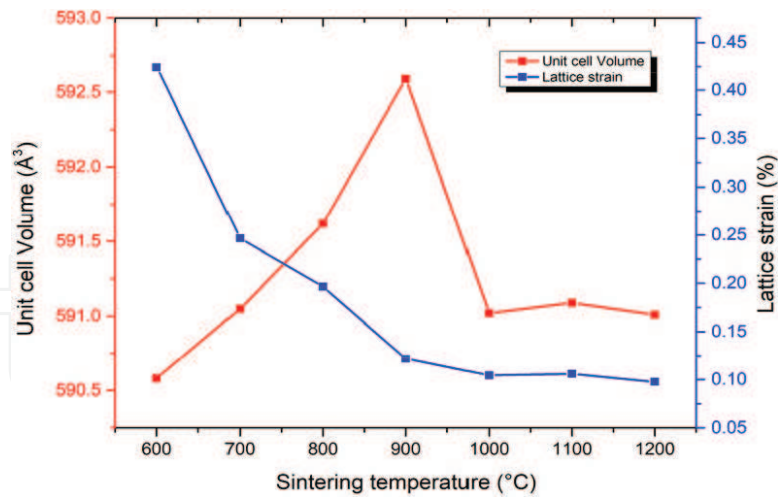
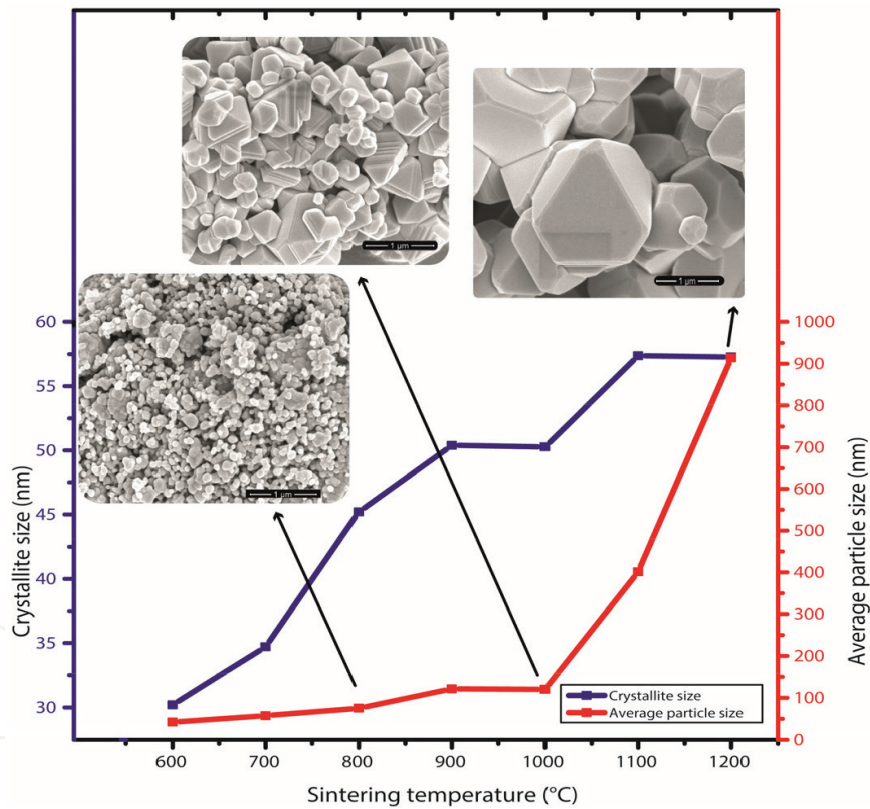**Figure 4.** Unit cell volume and lattice strain as a function of sintering temperature.

Figure 5. Average particle size and crystallite size as a function of sintering temperature; the evolution of morphology is shown in the inserted field emission scanning electron microscope (FESEM) micrographs.

Figure 5 shows the evolution of particle size, crystallite size, and morphological properties of $Ni_{0.5}Zn_{0.5}Fe_2O_4$ with elevating sintering temperature. As a whole, bottom-up synthesis of soft ferrite, $Ni_{0.5}Zn_{0.5}Fe_2O_4$ acquires three stages of sintering. Initial stage of sintering can be observed for samples sintered at 600-, 700-, and 800°C. Phenomena such as rearrangement

of particles and necking structure can be observed at this stage. At the intermediate stage (900-, 1000-, and 1100°C), further increase of sintering provides sufficient thermal energy for nanoparticles to move closer. Grain boundaries are formed. However, the most significant observation for intermediate stage is the formation of interconnected pores. Finally, the sample sintered at 1200°C exhibited the final stage of sintering. Isolated pores are observed, and rigid crystal structure is visible. The coarsening and densification of particles are observed with increasing sintering temperature.

6.2. Three stages of sintering

The activation energy of particle growth of sintering is strongly related to the size evolution of the particles [24]. Size-dependent activation energy can be represented by the plot of log particle size (*D*) versus the reciprocal of absolute temperature (*1/T*) of $Ni_{0.5}Zn_{0.5}Fe_2O_4$ [25]. Three distinct stages of sintering can be observed in **Figure 6**. Activation energy is the lowest at initial stage, indicating the particles are nano-sized, which exhibit relatively largest surface area. Small thermal energy is enough to initiate the particle growth. Through intermediate and final stages, particle size increases, therefore, the activation energy for particle growth increases hence higher thermal energy is required for the densification and coarsening mechanisms in sintering [26]. As a summary during initial stage, particles rearranged themselves so that they
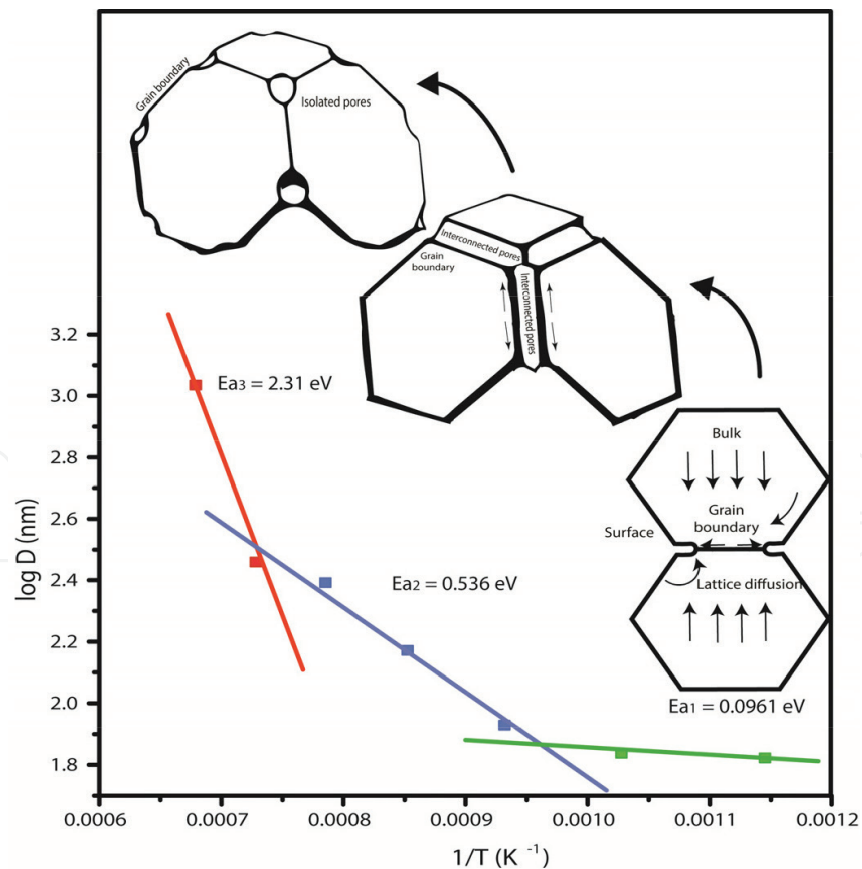

Figure 6. Plot of log D versus the reciprocal of absolute temperature (1/T) of $Ni_{0.5}Zn_{0.5}Fe_2O_4$ showing three stages of sintering.

are in tangential contact. This is to activate the material transport mechanism through diffusion. During this process, necking structures are formed between particles. At intermediate stage, densification occurs and the pores shrink to reduce their cross-section. As a result, interconnected pores are formed at the boundary regions. Densification and coarsening continue to occur; eventually, the pores become unstable and isolated at the final stage of sintering [1].

High resolution transmission electron microscopy (HRTEM) is utilized to identify some unique features of each stage in terms of atomic arrangement, structural information, and defects like grain boundaries. In **Figure 7a**, a lattice spacing of 2.53 Å was measured for $Ni_{0.5}Zn_{0.5}Fe_2O_4$, corresponding to (113) lattice plane. A few particles rearrange themselves in such a way that they are in tangential contact. The contact points between particles are the material transport paths that allow diffusions to occur at early stage of sintering. In **Figure 7b**, it can be seen that the spheres begin to coalesce. The radius of the necking structure has reached a value of >0.50 of the particle radius. This indicated that at sintering temperature of 800°C, the particles are near the end of an initial stage of sintering [1].

In **Figure 8a**, it can be observed that two particles were brought together, and they are undergoing deformation in response to surface energy reduction. Massive lattice diffusion and material transport occur between these particles. In **Figure 8b**, grains adopt the shape of polyhedron with multiple faces, and the edge of the particle appears to have a clean
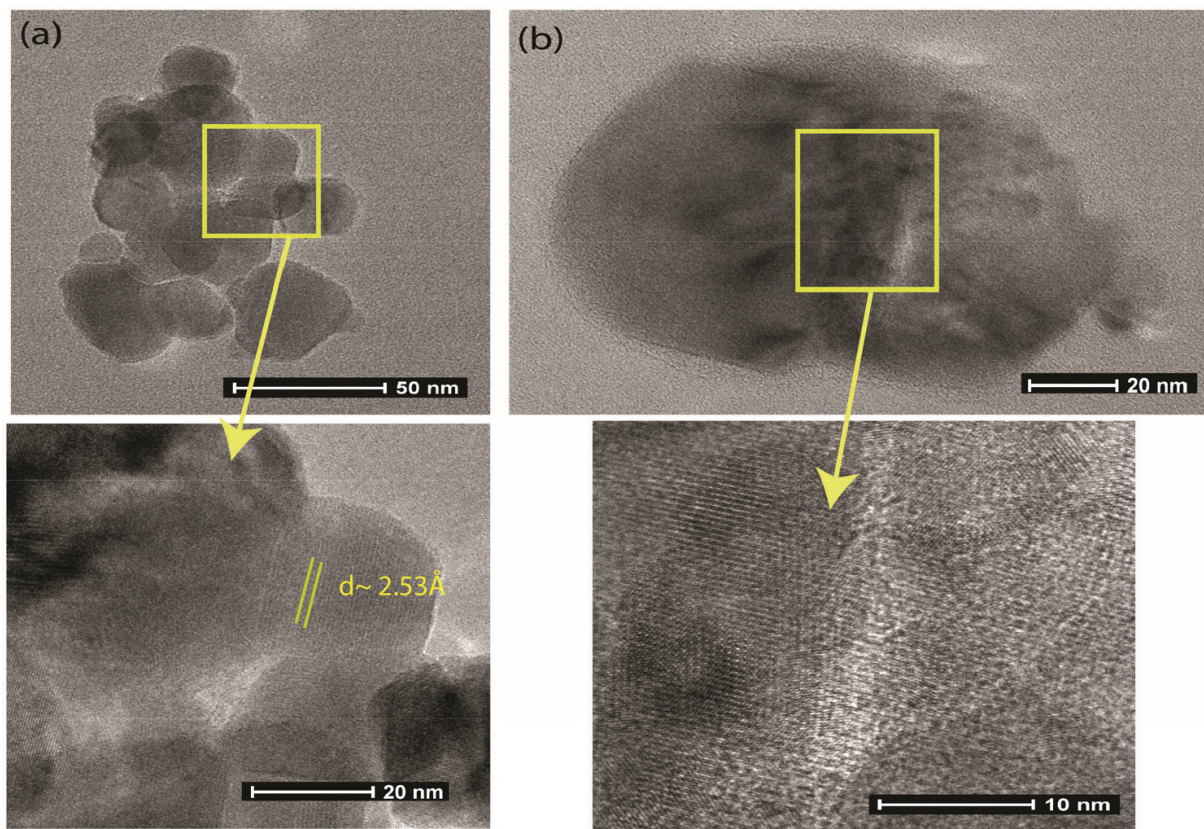

Figure 7. High resolution transmission electron microscopy (TEM) images for $Ni_{0.5}Zn_{0.5}Fe_2O_4$ nanoparticles sintered at (a) 600°C, and (b) 800°C (initial stage of sintering).

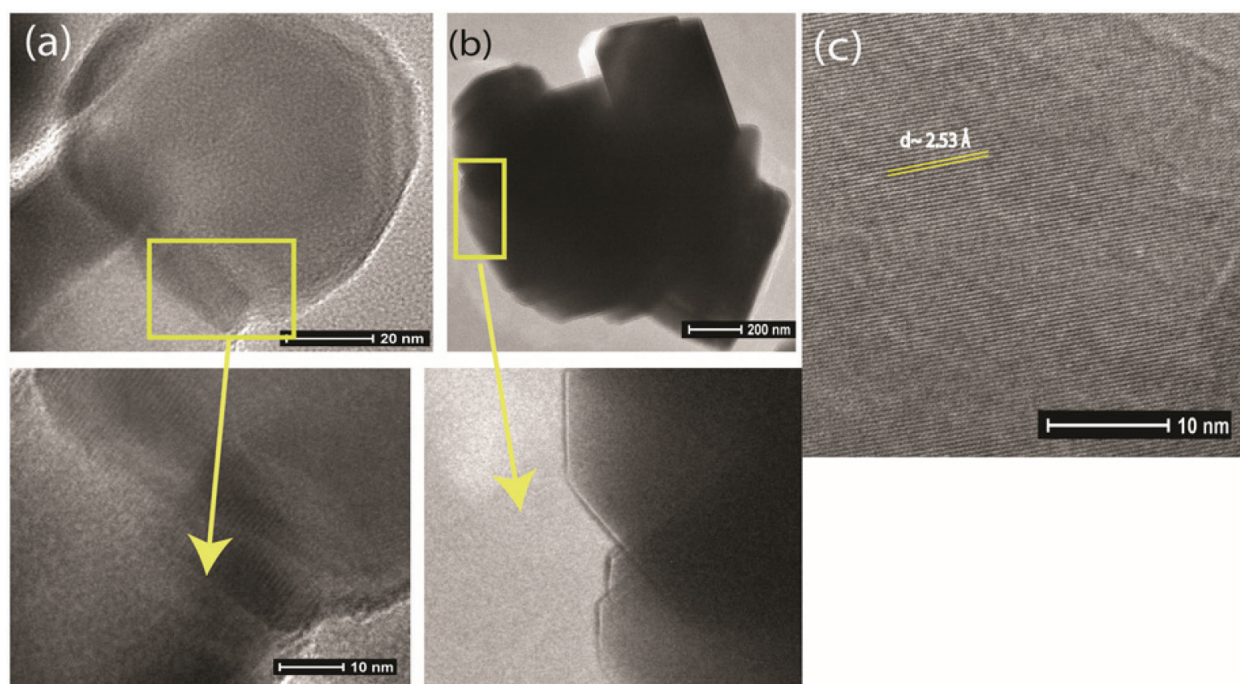**Figure 8.** High resolution TEM images for $Ni_{0.5}Zn_{0.5}Fe_2O_4$ nanoparticles sintered at (a) 900°C, (b) 1100°C (intermediate stage of sintering), and (c) 1200°C (final stage of sintering).

crystalline surface, where amorphous phase diminishes at 1100°C. In the final stage of sintering (**Figure 8c**), a homogeneous atomic arrangement, with (113) lattice plane is formed.

6.3. Microstructural related properties of sintered $Ni_{0.5}Zn_{0.5}Fe_2O_4$

Figure 9a shows the M-H hysteresis loops of $Ni_{0.5}Zn_{0.5}Fe_2O_4$ sintered at various temperatures. The magnetic parameters are extracted from hysteresis loops. All the samples sintered from 600 to 1200°C exhibited less slanting, narrow sigmoid hysteresis loop. This indicates that the preparation of raw powder with modified high-speed mechanical alloying increases the reactivity of nanoparticles. Ferromagnetic phase exists in the sample even at low sintering temperatures such as 600 and 700°C. **Figure 9b** shows the plot of maximum magnetization at 10 kOe, M_{10kOe} against sintering temperature. In view of the results obtained, the M_{10kOe} values increase with increasing sintering temperature. At low sintering temperature, small particles exhibit surface distortion due to the interaction of transition metal ions in the lattice with oxygen atoms, causing a reduction in the resultant magnetic moment. This phenomenon is normally predominant in ultrafine particles because of their large surface to volume ratio. This effect becomes less influential at high sintering temperature as particle size increases. Volume fraction of amorphous phase decreases with increasing sintering temperature. Thus, the exchange interaction between particles increases with increasing volume fraction of crystalline phase. As a result, strong ferromagnetic behaviors are strengthened with erect, narrow, and well-defined sigmoid hysteresis loops are observed with increasing temperature. Coercivity has an indirect relationship with particle size. At low sintering temperature, there are amorphous phase and defects like grain boundaries in the sample. Therefore, the magnetocrystalline anisotropy is low because the crystalline volume fraction is low. Below a critical size ($D_c \approx 90$ nm), coercivity increases with average particle size. As the sintering temperature increases, the crystalline volume fraction increases, the magnetocrystalline
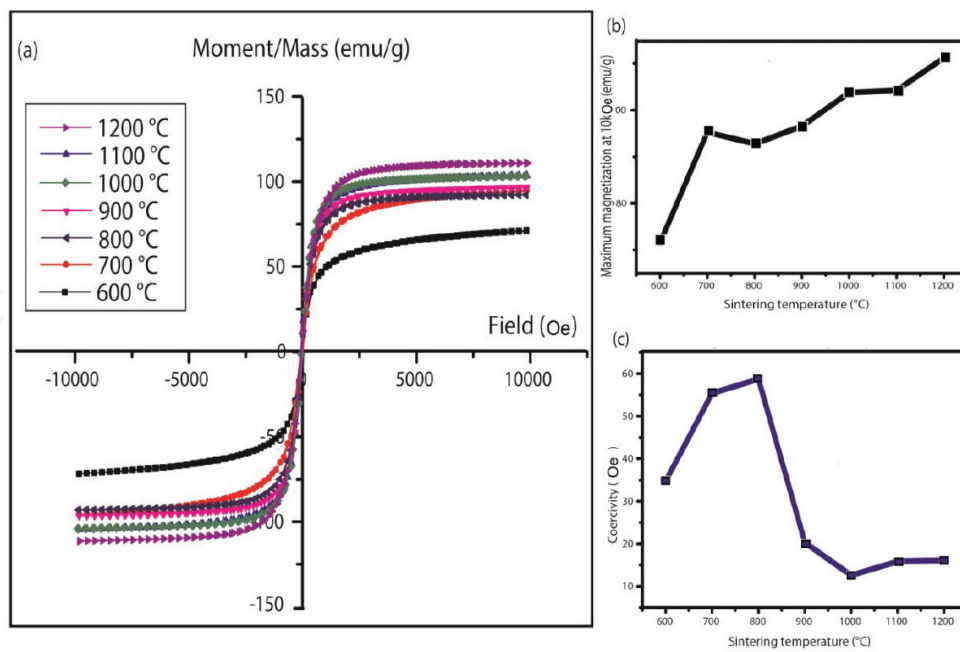
Figure 9. Magnetic parameters of bottom-up synthesis $Ni_{0.5}Zn_{0.5}Fe_2O_4$: (a) hysteresis loops at different sintering temperature, (b) plot of M_{10kOe} versus sintering temperature, (c) plot of coercivity versus sintering temperature.

anisotropy is enhanced. To change the orientation of magnetic moment, higher energy is required to overcome this magnetocrystalline anisotropy energy. Therefore, below D_c, coercivity increases with increasing average particle size. Above this D_c, high magnetocrystalline anisotropy is not favorable in terms of energy level [27]. In order to reduce the overall energy of the system, domain walls are created causing the coercivity to decrease.

In **Figure 10**, a red shift of optical property is observed with increasing sintering tempera-ture. It can be seen that the increase of crystallite is accompanied with the decrease of optical bandgap values (red-shift). This is thought to be due to size-dependent quantum confine-ment effect. Quantum confinement effect can be observed when the crystallite size is in the same order as the wavelength of the electron. The energy level at the microscopic level can be described by the expression [28]:

$$E = \frac{(hk)^2}{2m} \tag{5}$$

where h is the Planck constant, k is the wave factor ($k = 2\pi/\lambda$), m is the mass of electron. When the crystallite size is small, the wave vector k can be expressed as [28]:

$$k = \frac{2\pi}{\lambda} = \frac{n\pi}{a} \tag{6}$$

where a is the crystallite size of the material and n is an integer. Based on Eqs. 5 and 6, the value of wave vector k has an inversely proportional relationship with the crystallite size. The crystallite size increased with increasing sintering temperature resulting in decrease of wave vector k value. When we substitute n = 1, 2, 3, and so on, for Eqs. 5 and 6, the difference between two consecutive energy becomes smaller. Therefore, energy bandgap values decrease with increasing crystallite size. This phenomenon happens when the motion of electrons is restricted in a nano-scale size.
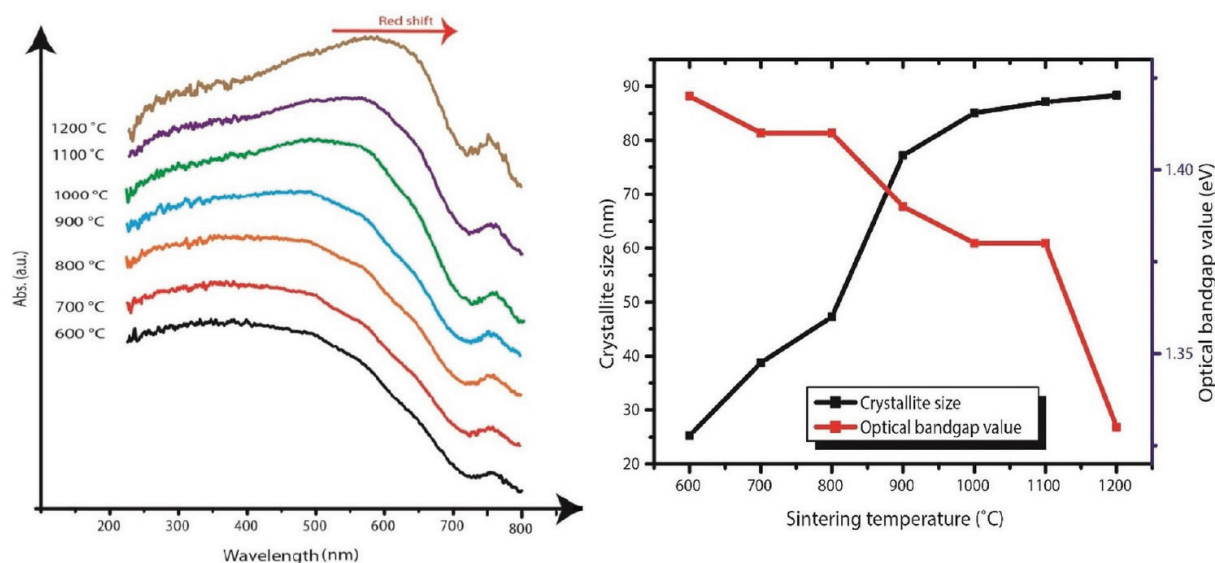
Figure 10. Optical properties of $Ni_{0.5}Zn_{0.5}Fe_2O_4$ nanoparticles sintered at different sintering temperature.

7. Comparative study of bottom-up and top-down approach synthesis

Sample with similar particle size, synthesized via mechanochemical process with optimized parameters [29] is chosen as a candidate for this comparative study with two parameters were chosen, which were milling at 8 hours (top-down approach) and sintering synthesis at 900°C (bottom-up approach). **Figure 11** shows the XRD diffraction patterns milled at 8 hours and sintered at 900°C $Ni_{0.5}Zn_{0.5}Fe_2O_4$ nanoparticles. Nanoparticles that milled 8 hours exhibit a superimposition of broad diffraction reflections on the broad diffraction maximum or "hump," indicating the presence of a highly disordered phase. Nanoparticles that sintered at 900°C exhibit a single phase pattern with sharp Braggs peaks.

Figure 12. shows the field emission scanning electron microscope (FESEM) micrographs and particle size distribution for nanoparticles synthesized by different synthesis approaches. As can be seen, nanoparticles that sintered at 900°C have a narrower size distribution compared to nanoparticles that milled at 8 hours. Commercial nanoparticles are uniform in size. Densification mechanism of sintering can be seen in **Figure 12b**. Small and large particles coexisted for both bottom-up and top-down approaches synthesized nanoparticles. However, particles with rigid and clear grain boundaries can be observed in sintered particles while top-down approach synthesized particles are agglomerated particles with randomly shaped boundaries.

Figure 13 shows the M-H hysteresis loops of $Ni_{0.5}Zn_{0.5}Fe_2O_4$ nanoparticles synthesized via different synthesis approaches. Nanoparticles that milled at 8 hours exhibited complex disordering in structure. Therefore, it possesses canted spin arrangement that has significant implications on its magnetism. The maximum magnetization at 10 kOe is lower compared to nanoparticles that sintered at 900°C. On the other hand, nanoparticles that sintered at 900°C exhibited low coercivity with high saturation magnetization (the magnetization at 10 kOe had
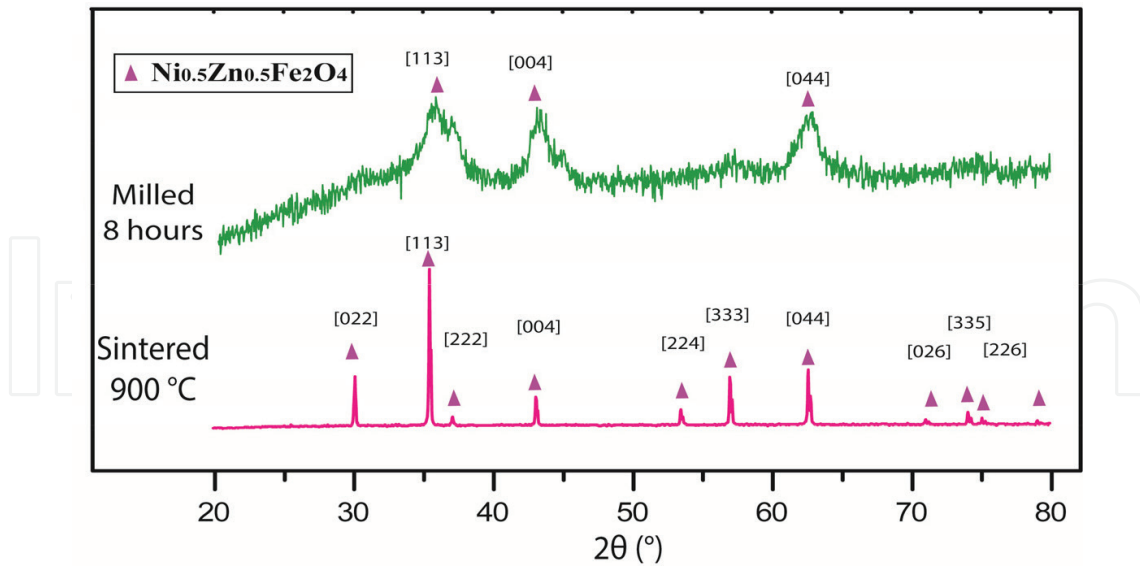
Figure 11. X-ray diffraction patterns of $Ni_{0.5}Zn_{0.5}Fe_2O_4$ nanoparticles synthesized by different synthesis approaches.
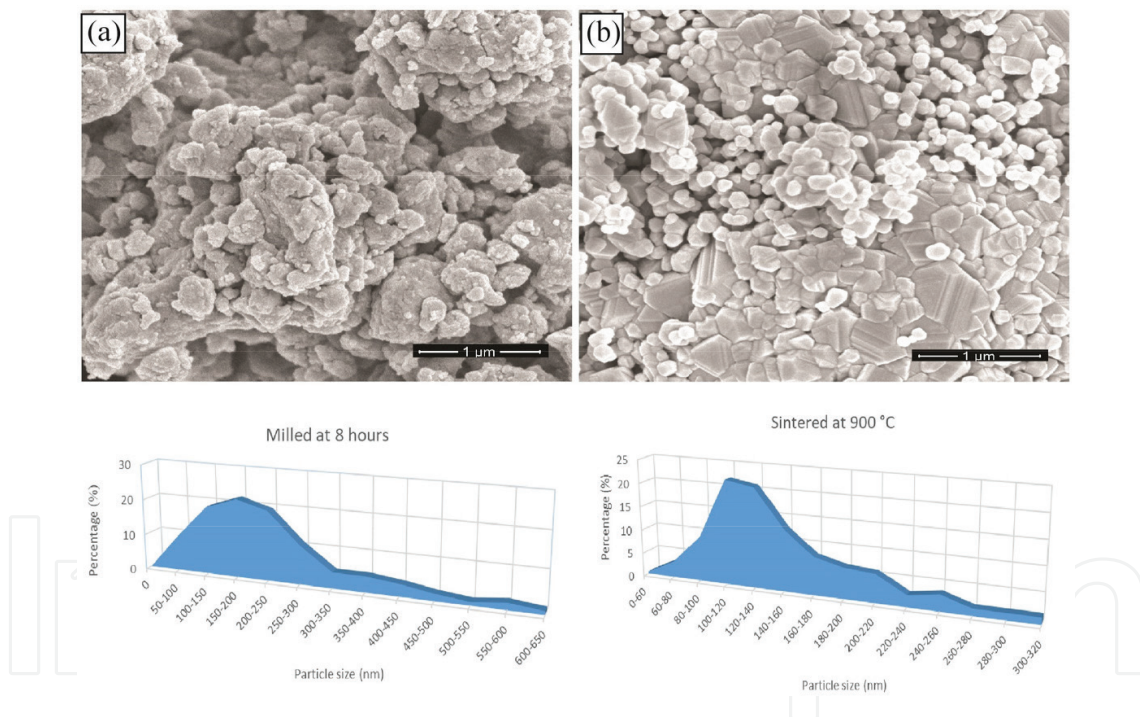

Figure 12. FESEM micrographs and particle size distribution for (a) milled at 8 hours and (b) sintered at 900°C.

saturated). This indicated that the formation of single phase nickel zinc ferrite that exhibits soft ferrite magnetic properties. The optical bandgap values were 1.39–1.30 eV for sintered at 900°C and milled at 8 hours nanoparticles, respectively. Both bottom-up and top-down approaches synthesized nanoparticles exhibit same order optical bandgap value. It is evident that optical bandgap is a size-dependent behavior. However, defects that induced during mechanochemical process reduced the optical bandgap value of nanoparticles that milled at 8 hours. This is attributed to structural disorder bandgap narrowing effect.
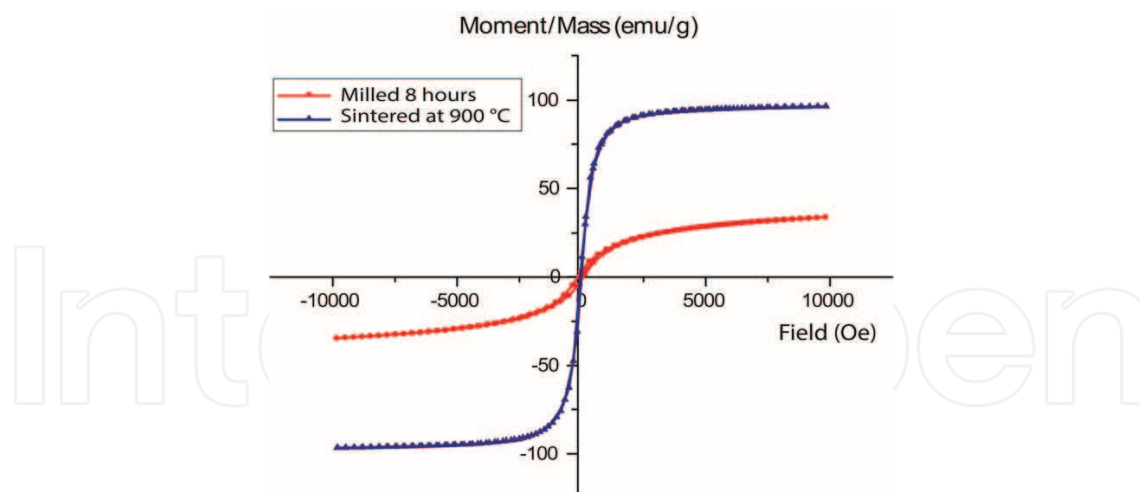
Figure 13. M-H hysteresis loops of $Ni_{0.5}Zn_{0.5}Fe_2O_4$ nanoparticles synthesized by different synthesis approaches.

8. Conclusions

As most common approach for the fabrication of ceramic material, sintering shows some irreplaceable advantages. Sintering provides control on processing variables like sintering temperature, to achieve required microstructure for a particular set of properties. The synthesis temperature for single homogeneous phase can be lowered by mechanically activates the starting materials. Three stages of sintering mechanism can be observed in the experimental data of Ni-Zn ferrite. The observed evolutional relationship between microstructural, magnetic, and optical properties can be used to develop a useful framework for designing a sintering condition for final microstructure with desired properties. From the comparative study of top-down and bottom-up approaches carried out, we concluded that different synthesis methods produced ceramic materials with different behaviors. Top-down approach synthesis method has the ability to produce nanocrystalline particles, which then must be compacted without losing the refined microstructural properties, with high uniformity in terms of size, and morphological properties. This remains a challenge to this approach otherwise it is a versatile method. Bottom-up approach synthesis method is capable of producing particles with refined microstructures, which then high-purity single phase particles must be produced with particle size below 100 nm. This is relatively more difficult as single phase can only be achieved when sufficient heat energy is provided, and typically single phase particles are produced at high sintering temperature where particle growth is unavoidable.

Acknowledgements

Author details

Zhi Huang Low[1], Ismayadi Ismail[1]* and Kim Song Tan[2]

*Address all correspondence to: ismayadi@upm.edu.my

1 Materials Synthesis and Characterization Laboratory, Institute of Advanced Technology, Universiti Putra, Malaysia, Serdang, Selangor Darul Ehsan, Malaysia

2 Advanced Imaging Centre, Malaysian Rubber Board, RRIM Sungai Buloh, Selangor, Malaysia

References

[1] Rahaman MN. Sintering of Ceramics. Boca Raton: CRC Press; 2007

[2] Sopicka-Lizer M. High-Energy Ball Milling Mechanochemical Processing of Nanopowders. Boca Raton, Florida: CRC Press; 2010

[3] Holdren JP. Science and technology for sustainable well-being. Science. 2008;**319**:424-434

[4] Goldman A. Modern Ferrite Technology. 2nd ed. Pittsburgh, PA, USA: Springer; 2006

[5] Idza IR, Hashim M, Rodziah N, Ismayadi I, Norailiana AR. Influence of evolving microstructure on magnetic-hysteresis characteristics in polycrystalline nickel–zinc ferrite, $Ni_{0.3}Zn_{0.7}Fe_2O_4$. Materials Research Bulletin. 2012;**47**(6):1345-1352

[6] Rodziah N, Hashim M, Idza IR, Ismayadi I, Hapishah AN, Khamirul MA. Applied surface science dependence of developing magnetic hysteresis characteristics on stages of evolving microstructure in polycrystalline yttrium iron garnet. Applied Surface Science. 2012;**258**(7):2679-2685

[7] Shafie MSE, Hashim M, Ismail I, Kanagesan S, Fadzidah MI, Idza IR, Hajalilou A, Sabbaghizadeh R. Magnetic M–H loops family characteristics in the microstructure evolution of $BaFe_{12}O_{19}$. Journal of Materials Science: Materials in Electronics. 2014;**25**(9): 3787-3794

[8] Ismail I, Hashim M, Matori KA, Alias R, Hassan J. The transition from paramagnetic to ferromagnetic states as influenced by evolving microstructure of $Ni_{0.5}Zn_{0.5}Fe_2O_4$. Journal of Superconductivity and Novel Magnetism. 2012;**25**(1):71-77

[9] Bera J, Roy PK. Effect of grain size on electromagnetic properties of $Ni_{0.7}Zn_{0.3}Fe_2O_4$ ferrite. Physica B: Condensed Matter. 2005;**363**(1-4):128-132

[10] Igarashi H, Okazaki K. Effects of porosity and grain size on the magnetic properties of NiZn ferrite. Journal of the American Ceramic Society. 1977;**60**(1-2):51-54

[11] Kingery WD. Plausible concepts necessary and sufficient for interpretation of ceramic grain-boundary phenomena: I, grain-boundary characteristics, structure, and electrostatic potential. Journal of the American Ceramic Society. 1974;**57**(1):1-8

[12] Dho J, Lee EK, Park JY, Hur NH. Effects of the grain boundary on the coercivity of barium ferrite BaFe$_{12}$O$_{19}$. Journal of Magnetism and Magnetic Materials. 2005;**285**(1-2):164-168

[13] Rikukawa H. Relationship between microstructures and magnetic properties of ferrites containing closed pores. IEEE Transactions on Magnetics. 1982;**18**(6):1535-1537

[14] Ibrahim IR, Hashim M, Nazlan R, Ismail I, Wan Ab Rahman WN, Abdullah NH, Idris FM, Shafie MSE, Zulkimi MMM. Grouping trends of magnetic permeability components in their parallel evolution with microstructure in Ni$_{0.3}$Zn$_{0.7}$Fe$_2$O$_4$. Journal of Magnetism and Magnetic Materials. 2014;**355**:265-275

[15] Suryanarayana C. Mechanical Alloying and Milling. New York: Marcel Dekker; 2004

[16] Benito G, Morales MP, Requena J, Raposo V, Vázquez M, Moya JS. Barium hexaferrite monodispersed nanoparticles prepared by the ceramic method. Journal of Magnetism and Magnetic Materials. 2001;**234**(1):65-72

[17] Zahi S, Daud AR, Hashim M. A comparative study of nickel-zinc ferrites by sol-gel route and solid-state reaction. Materials Chemistry and Physics. 2007;**106**(2-3):452-456

[18] Hajalilou A, Hashim M, Ebrahimi-Kahrizsangi R, Kamari HM. Influence of evolving microstructure on electrical and magnetic characteristics in mechanically synthesized polycrystalline Ni-ferrite nanoparticles. Journal of Alloys and Compounds. 2015;**633**: 306-316

[19] Low ZH, Hashim M, Ismail I, Kanagesan S, Ezzad Shafie MS, Idris FM, Ibrahim IR. Development of magnetic B-H hysteresis loops through stages of microstructure evolution of bulk BaFe$_{12}$O$_{19}$. Journal of Superconductivity and Novel Magnetism. 2015;**28**(10): 3075-3086

[20] Yan W, Li Q, Zhong H, Zhong Z. Characterization and low-temperature sintering of Ni$_{0.5}$Zn$_{0.5}$Fe$_2$O$_4$ nano-powders prepared by refluxing method. Powder Technology. 2009;**192**(1):23-26

[21] Zahi S, Hashim M, Daud AR. Synthesis, magnetic properties and microstructure of Ni-Zn ferrite by sol-gel technique. Journal of Magnetism and Magnetic Materials. 2007; **308**(2):177-182

[22] Chen DG, Tang XG, Wu JB, Zhang W, Liu QX, Jiang YP. Effect of grain size on the magnetic properties of superparamagnetic Ni$_{0.5}$Zn$_{0.5}$Fe$_2$O$_4$ nanoparticles by co-precipitation process. Journal of Magnetism and Magnetic Materials. 2011;**323**(12):1717-1721

[23] Cullity BD, Stock SR. Elements of X-Ray Diffraction. 3rd ed. United Kingdom: Pearson, Prentice Hall; 2011

[24] Phuoc TX, Chen R-H. Modeling the effect of particle size on the activation energy and ignition temperature of metallic nanoparticles. Combustion and Flame. 2012;**159**(1):416-419

[25] Jarcho M, Bolen CH, Thomas MB, Bobick J, Kay JF, Doremus RH. Hydroxylapatite synthesis and characterization in sense polycristalline forms. Journal of Materials Science. 1976;**11**:2027-2035

[26] Kang SJL. Sintering Densification, Grain Growth, and Microstructure. London, United Kingdom: Elsevier; 2005

[27] Skomski R, Sellmyer DJ. Intrinsic and extrinsic properties of advanced magnetic materials. ChemInform. 2006;**37**(47):1

[28] Fox M. Optical Properties of Solids. 2nd ed. United States: Clarendon Press Oxford; 2010

[29] Low ZH, Chen SK, Ismail I, Tan KS, Liew JYC. Structural transformations of mechanically induced top-down approach $BaFe_{12}O_{19}$ nanoparticles synthesized from high crystallinity bulk materials. Journal of Magnetism and Magnetic Materials. 2017;**429**:192-202